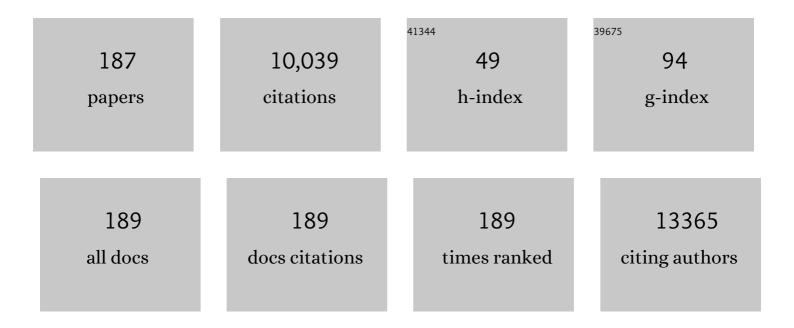
List of Publications by Year in descending order

Source: https://exaly.com/author-pdf/5137408/publications.pdf Version: 2024-02-01



HEE-TAE LUNC

#	Article	IF	CITATIONS
1	Metallic Ti ₃ C ₂ T _{<i>x</i>} MXene Gas Sensors with Ultrahigh Signal-to-Noise Ratio. ACS Nano, 2018, 12, 986-993.	14.6	1,153
2	Highly Enhanced Gas Adsorption Properties in Vertically Aligned MoS ₂ Layers. ACS Nano, 2015, 9, 9314-9321.	14.6	417
3	Superior Chemical Sensing Performance of Black Phosphorus: Comparison with MoS ₂ and Graphene. Advanced Materials, 2016, 28, 7020-7028.	21.0	355
4	Tunable Volatile Organic Compounds Sensor by Using Thiolated Ligand Conjugation on MoS ₂ . Nano Letters, 2014, 14, 5941-5947.	9.1	331
5	An investigation into the factors governing the oxidation of two-dimensional Ti ₃ C ₂ MXene. Nanoscale, 2019, 11, 8387-8393.	5.6	276
6	Evaluation of mechanical interlock effect on adhesion strength of polymer–metal interfaces using micro-patterned surface topography. International Journal of Adhesion and Adhesives, 2010, 30, 408-417.	2.9	265
7	Direct visualization of large-area graphene domains and boundaries by optical birefringency. Nature Nanotechnology, 2012, 7, 29-34.	31.5	222
8	High mass loading, binder-free MXene anodes for high areal capacity Li-ion batteries. Electrochimica Acta, 2015, 163, 246-251.	5.2	204
9	Selective Molecular Separation on Ti ₃ C ₂ T <i>_x</i> –Graphene Oxide Membranes during Pressure-Driven Filtration: Comparison with Graphene Oxide and MXenes. ACS Applied Materials & Interfaces, 2017, 9, 44687-44694.	8.0	193
10	Z-scheme Photocatalytic CO ₂ Conversion on Three-Dimensional BiVO ₄ /Carbon-Coated Cu ₂ O Nanowire Arrays under Visible Light. ACS Catalysis, 2018, 8, 4170-4177.	11.2	190
11	Amine-Functionalized Graphene/CdS Composite for Photocatalytic Reduction of CO ₂ . ACS Catalysis, 2017, 7, 7064-7069.	11.2	189
12	In Situ Formation of Multiple Schottky Barriers in a Ti ₃ C ₂ MXene Film and its Application in Highly Sensitive Gas Sensors. Advanced Functional Materials, 2020, 30, 2003998.	14.9	187
13	Internal structure visualization and lithographic use of periodic toroidal holes in liquid crystals. Nature Materials, 2007, 6, 866-870.	27.5	179
14	High-Resolution p-Type Metal Oxide Semiconductor Nanowire Array as an Ultrasensitive Sensor for Volatile Organic Compounds. Nano Letters, 2016, 16, 4508-4515.	9.1	156
15	Preparation of graphene relying on porphyrin exfoliation of graphite. Chemical Communications, 2010, 46, 5091.	4.1	154
16	Enhanced Selectivity of MXene Gas Sensors through Metal Ion Intercalation: In Situ X-ray Diffraction Study. ACS Sensors, 2019, 4, 1365-1372.	7.8	154
17	Immobilization-free screening of aptamers assisted by graphene oxide. Chemical Communications, 2012, 48, 2071-2073.	4.1	149
18	An Ultrasensitive, Viscoâ€Poroelastic Artificial Mechanotransducer Skin Inspired by Piezo2 Protein in Mammalian Merkel Cells. Advanced Materials, 2017, 29, 1605973.	21.0	147

#	Article	IF	CITATIONS
19	Enhanced Stability of Laminated Graphene Oxide Membranes for Nanofiltration via Interstitial Amide Bonding. ACS Applied Materials & Interfaces, 2016, 8, 27376-27382.	8.0	128
20	Tunable Volatile-Organic-Compound Sensor by Using Au Nanoparticle Incorporation on MoS ₂ . ACS Sensors, 2017, 2, 183-189.	7.8	118
21	Tunable Chemical Sensing Performance of Black Phosphorus by Controlled Functionalization with Noble Metals. Chemistry of Materials, 2017, 29, 7197-7205.	6.7	117
22	Ultrasensitive Detection of VOCs Using a Highâ€Resolution CuO/Cu ₂ O/Ag Nanopattern Sensor. Advanced Functional Materials, 2019, 29, 1808319.	14.9	117
23	Springtail-inspired superomniphobic surface with extreme pressure resistance. Science Advances, 2018, 4, eaat4978.	10.3	112
24	Highly Efficient and Stable CO ₂ Reduction Photocatalyst with a Hierarchical Structure of Mesoporous TiO ₂ on 3D Graphene with Few-Layered MoS ₂ . ACS Sustainable Chemistry and Engineering, 2018, 6, 5718-5724.	6.7	110
25	Enhanced diode characteristics of organic solar cells using titanium suboxide electron transport layer. Applied Physics Letters, 2010, 96, .	3.3	104
26	Continuous Meter-Scale Synthesis of Weavable Tunicate Cellulose/Carbon Nanotube Fibers for High-Performance Wearable Sensors. ACS Nano, 2019, 13, 9332-9341.	14.6	103
27	Etching Mechanism of Monoatomic Aluminum Layers during MXene Synthesis. Chemistry of Materials, 2021, 33, 6346-6355.	6.7	102
28	Smectic Liquid Crystal Defects for Selfâ€Assembling of Building Blocks and Their Lithographic Applications. Advanced Functional Materials, 2011, 21, 610-627.	14.9	94
29	Pore-Size-Tuned Graphene Oxide Frameworks as Ion-Selective and Protective Layers on Hydrocarbon Membranes for Vanadium Redox-Flow Batteries. Nano Letters, 2018, 18, 3962-3968.	9.1	93
30	Interfacial Assembly of Ultrathin, Functional MXene Films. ACS Applied Materials & Interfaces, 2019, 11, 32320-32327.	8.0	91
31	Cu/Cu ₂ 0 Interconnected Porous Aerogel Catalyst for Highly Productive Electrosynthesis of Ethanol from CO ₂ . Advanced Functional Materials, 2021, 31, 2102142.	14.9	90
32	Bulk scale growth of CVD graphene on Ni nanowire foams for a highly dense and elastic 3D conducting electrode. Carbon, 2014, 80, 446-452.	10.3	89
33	From Vesicle Size Distributions to Bilayer Elasticity via Cryo-Transmission and Freeze-Fracture Electron Microscopy. Langmuir, 2003, 19, 5632-5639.	3.5	86
34	A highly photoactive, visible-light-driven graphene/2D mesoporous TiO ₂ photocatalyst. Green Chemistry, 2015, 17, 3972-3978.	9.0	84
35	Intercalation of Gas Molecules in Graphene Oxide Interlayer: The Role of Water. Journal of Physical Chemistry C, 2014, 118, 11142-11148.	3.1	83
36	Ultrasmall Grained Pd Nanopattern H ₂ Sensor. ACS Sensors, 2018, 3, 1876-1883.	7.8	79

#	Article	IF	CITATIONS
37	High quality reduced graphene oxide through repairing with multi-layered graphene ball nanostructures. Scientific Reports, 2013, 3, 3251.	3.3	76
38	An Ultrastable Ionic Chemiresistor Skin with an Intrinsically Stretchable Polymer Electrolyte. Advanced Materials, 2018, 30, e1706851.	21.0	75
39	Confined Self-Assembly of Toric Focal Conic Domains (The Effects of Confined Geometry on the) Tj ETQq1 1 0.7	84314 rgB 3.5	T /Overlock
40	New Top-Down Approach for Fabricating High-Aspect-Ratio Complex Nanostructures with 10 nm Scale Features. Nano Letters, 2010, 10, 3604-3610.	9.1	71
41	Enhanced water permeation based on nanoporous multilayer graphene membranes: the role of pore size and density. Journal of Materials Chemistry A, 2016, 4, 17773-17781.	10.3	71
42	Sulfur infiltrated mesoporous graphene–silica composite as a polysulfide retaining cathode material for lithium–sulfur batteries. Carbon, 2014, 69, 543-551.	10.3	64
43	Ultrafast-Selective Nanofiltration of an Hybrid Membrane Comprising Laminated Reduced Graphene Oxide/Graphene Oxide Nanoribbons. ACS Applied Materials & Interfaces, 2019, 11, 27004-27010.	8.0	63
44	Well-Defined and High Resolution Pt Nanowire Arrays for a High Performance Hydrogen Sensor by a Surface Scattering Phenomenon. Analytical Chemistry, 2015, 87, 1480-1484.	6.5	58
45	Electrical Conductivity of Graphene Films with a Poly(allylamine hydrochloride) Supporting Layer. Langmuir, 2009, 25, 11008-11013.	3.5	57
46	Optically Selective Microlens Photomasks Using Selfâ€Assembled Smectic Liquid Crystal Defect Arrays. Advanced Materials, 2010, 22, 2416-2420.	21.0	57
47	Recent Progress in Simple and Costâ€Effective Topâ€Down Lithography for â‰^10 nm Scale Nanopatterns: From Edge Lithography to Secondary Sputtering Lithography. Advanced Materials, 2020, 32, e1907101.	21.0	57
48	Ambient Stabilization of Few Layer Phosphorene via Noncovalent Functionalization with Surfactants: Systematic 2D NMR Characterization in Aqueous Dispersion. Chemistry of Materials, 2019, 31, 2786-2794.	6.7	54
49	Flexible Two-Dimensional Ti ₃ C ₂ MXene Films as Thermoacoustic Devices. ACS Nano, 2019, 13, 12613-12620.	14.6	53
50	Graphene Oxide/Carbon Nanotube Bilayer Flexible Membrane for Highâ€Performance Li–S Batteries with Superior Physical and Electrochemical Properties. Advanced Materials Interfaces, 2019, 6, 1801992.	3.7	53
51	Universal Method for Creating Hierarchical Wrinkles on Thin-Film Surfaces. ACS Applied Materials & Interfaces, 2018, 10, 1347-1355.	8.0	49
52	Synthesis of SWNT Rings by Noncovalent Hybridization of Porphyrins and Single-Walled Carbon Nanotubes. Journal of Physical Chemistry C, 2008, 112, 12264-12271.	3.1	46
53	High Facets on Nanowrinkled Cu via Chemical Vapor Deposition Graphene Growth for Efficient CO ₂ Reduction into Ethanol. ACS Catalysis, 2021, 11, 5658-5665.	11.2	46
54	Fabrication of two-dimensional dimple and conical microlens arrays from a highly periodic toroidal-shaped liquid crystal defect array. Journal of Materials Chemistry, 2010, 20, 6557.	6.7	45

#	Article	IF	CITATIONS
55	Monolithic Polymer Nanoridges with Programmable Wetting Transitions. Advanced Materials, 2018, 30, e1706657.	21.0	45
56	Synergistic Effect of Cu ₂ O Mesh Pattern on Highâ€Facet Cu Surface for Selective CO ₂ Electroreduction to Ethanol. Advanced Materials, 2022, 34, e2106028.	21.0	44
57	Role of 1D Metallic Nanowires in Polydomain Graphene for Highly Transparent Conducting Films. Advanced Materials, 2014, 26, 4575-4581.	21.0	43
58	A three-dimensional metal grid mesh as a practical alternative to ITO. Nanoscale, 2016, 8, 14257-14263.	5.6	43
59	Ultrafast Interfacial Self-Assembly of 2D Transition Metal Dichalcogenides Monolayer Films and Their Vertical and In-Plane Heterostructures. ACS Applied Materials & Interfaces, 2017, 9, 1021-1028.	8.0	43
60	Bifunctional ITO layer with a high resolution, surface nano-pattern for alignment and switching of LCs in device applications. NPG Asia Materials, 2012, 4, e7-e7.	7.9	42
61	Fabrication of enzyme-based coatings on intact multi-walled carbon nanotubes as highly effective electrodes in biofuel cells. Scientific Reports, 2017, 7, 40202.	3.3	42
62	Self-assembled periodic liquid crystal defects array for soft lithographic template. Soft Matter, 2010, 6, 1426.	2.7	41
63	Edge-Functionalized Graphene Nanoribbon Chemical Sensor: Comparison with Carbon Nanotube and Graphene. ACS Applied Materials & Interfaces, 2018, 10, 42905-42914.	8.0	41
64	Multiarray Nanopattern Electronic Nose (Eâ€Nose) by Highâ€Resolution Topâ€Đown Nanolithography. Advanced Functional Materials, 2020, 30, 2002486.	14.9	40
65	Finding Hidden Signals in Chemical Sensors Using Deep Learning. Analytical Chemistry, 2020, 92, 6529-6537.	6.5	40
66	Relationship between Hydrogen Evolution and Wettability for Multiscale Hierarchical Wrinkles. ACS Applied Materials & Interfaces, 2019, 11, 7546-7552.	8.0	39
67	Highly Enhanced Fluorescence Signals of Quantum Dot–Polymer Composite Arrays Formed by Hybridization of Ultrathin Plasmonic Au Nanowalls. Nano Letters, 2015, 15, 7273-7280.	9.1	38
68	Large-Area Buckled MoS ₂ Films on the Graphene Substrate. ACS Applied Materials & Interfaces, 2016, 8, 13512-13519.	8.0	38
69	Polyelemental Nanolithography via Plasma Ion Bombardment: From Fabrication to Superior H ₂ Sensing Application. Advanced Materials, 2019, 31, e1805343.	21.0	38
70	Polyelemental Nanoparticles as Catalysts for a Li–O ₂ Battery. ACS Nano, 2021, 15, 4235-4244.	14.6	38
71	Recent advances in the fabrication of nanotemplates from supramolecular self-organization. Journal of Materials Chemistry, 2009, 19, 9091.	6.7	37
72	Turbostratic nanoporous carbon sheet membrane for ultrafast and selective nanofiltration in viscous green solvents. Journal of Materials Chemistry A, 2020, 8, 8292-8299.	10.3	37

#	Article	IF	CITATIONS
73	Enhanced nanofiltration performance of graphene-based membranes on wrinkled polymer supports. Carbon, 2019, 148, 370-377.	10.3	36
74	Molybdenum carbide chemical sensors with ultrahigh signal-to-noise ratios and ambient stability. Journal of Materials Chemistry A, 2018, 6, 23408-23416.	10.3	35
75	Ultrathin graphene oxide membranes on freestanding carbon nanotube supports for enhanced selective permeation in organic solvents. Scientific Reports, 2018, 8, 1959.	3.3	34
76	A High Aspect Ratio Serpentine Structure for Use As a Strainâ€Insensitive, Stretchable Transparent Conductor. Small, 2018, 14, 1702818.	10.0	32
77	Revealing the Role of Oxygen Debris and Functional Groups on the Water Flux and Molecular Separation of Graphene Oxide Membrane: A Combined Experimental and Theoretical Study. Journal of Physical Chemistry C, 2018, 122, 17507-17517.	3.1	32
78	Ultraclean transfer of CVD-grown graphene and its application to flexible organic photovoltaic cells. Journal of Materials Chemistry A, 2014, 2, 20474-20480.	10.3	31
79	Simultaneously Induced Selfâ€Assembly of Poly(3â€hexylthiophene) (P3HT) Nanowires and Thinâ€Film Fabrication via Solutionâ€Floating Method on a Water Substrate. Advanced Materials Interfaces, 2017, 4, 1700342.	3.7	31
80	Distinct Mechanosensing of Human Neural Stem Cells on Extremely Limited Anisotropic Cellular Contact. ACS Applied Materials & Interfaces, 2018, 10, 33891-33900.	8.0	31
81	The Present and Future of Gas Sensors. ACS Sensors, 2022, 7, 912-913.	7.8	28
82	Three-dimensional textures and defects of soft material layering revealed by thermal sublimation. Proceedings of the National Academy of Sciences of the United States of America, 2013, 110, 19263-19267.	7.1	27
83	Fabrication of 10 nm-Scale Complex 3D Nanopatterns with Multiple Shapes and Components by Secondary Sputtering Phenomenon. ACS Nano, 2014, 8, 1204-1212.	14.6	27
84	One dimensional building blocks for molecular separation: laminated graphitic nanoribbons. Nanoscale, 2017, 9, 19114-19123.	5.6	27
85	Ten Nanometer Scale WO ₃ /CuO Heterojunction Nanochannel for an Ultrasensitive Chemical Sensor. Analytical Chemistry, 2019, 91, 6850-6858.	6.5	27
86	Evaluation of highly stable ultrahigh-molecular-weight partially hydrolyzed polyacrylamide for enhanced oil recovery. Macromolecular Research, 2015, 23, 518-524.	2.4	26
87	Complex Highâ€Aspectâ€Ratio Metal Nanostructures by Secondary Sputtering Combined with Block Copolymer Selfâ€Assembly. Advanced Materials, 2016, 28, 8439-8445.	21.0	26
88	Scalable Superior Chemical Sensing Performance of Stretchable Ionotronic Skin via a Ï€â€Hole Receptor Effect. Advanced Materials, 2021, 33, e2007605.	21.0	25
89	Surface Ordering of a Perfluorinated, Self-Assembled, Dendrimer on a Water Subphase. Langmuir, 2005, 21, 4989-4995.	3.5	24
90	Macroscopic alignment of chromonic liquid crystals using patterned substrates. Physical Chemistry Chemical Physics, 2016, 18, 10362-10366.	2.8	24

#	Article	IF	CITATIONS
91	Extraordinary dendrite-free Li deposition on highly uniform facet wrinkled Cu substrates in carbonate electrolytes. Nano Energy, 2021, 82, 105736.	16.0	24
92	Generation of high-density nanoparticles in the carbothermal shock method. Science Advances, 2021, 7, eabk2984.	10.3	23
93	Combining the silver nanowire bridging effect with chemical doping for highly improved conductivity of CVD-grown graphene films. Journal of Materials Chemistry C, 2014, 2, 5902.	5.5	22
94	Periodic arrays of liquid crystalline torons in microchannels. RSC Advances, 2015, 5, 19279-19283.	3.6	22
95	Understanding Reaction Pathways in High Dielectric Electrolytes Using β-Mo ₂ C as a Catalyst for Li–CO ₂ Batteries. ACS Applied Materials & Interfaces, 2020, 12, 32633-32641.	8.0	22
96	Liquid-crystal periodic zigzags from geometrical and surface-anchoring-induced confinement: Origin and internal structure from mesoscopic scale to molecular level. Physical Review E, 2010, 82, 041705.	2.1	21
97	Vertically Aligned Nanopatterns of Amineâ€Functionalized Ti ₃ C ₂ MXene via Soft Lithography. Advanced Materials Interfaces, 2020, 7, 2000424.	3.7	20
98	N–p-Conductor Transition of Gas Sensing Behaviors in Mo ₂ CT _{<i>x</i>} MXene. ACS Sensors, 2022, 7, 2225-2234.	7.8	20
99	Synthesis and Device Performance of a Highly Efficient Fluorene-Based Blue Emission Polymer Containing Bulky 9,9-Dialkylfluorene Substituents. Macromolecules, 2009, 42, 6339-6347.	4.8	19
100	Surface plasmon assisted high performance top-illuminated polymer solar cells with nanostructured Ag rear electrodes. Journal of Materials Chemistry A, 2014, 2, 2915.	10.3	19
101	Direct Observation of Highly Ordered Dendrimer Soft Building Blocks over a Large Area. Nano Letters, 2015, 15, 7552-7557.	9.1	19
102	Facile Fabrication of High-Definition Hierarchical Wrinkle Structures for Investigating the Geometry-Sensitive Fate Commitment of Human Neural Stem Cells. ACS Applied Materials & Interfaces, 2019, 11, 17247-17255.	8.0	19
103	Ternary Hybrid Aerogels of g ₃ N ₄ /αâ€Fe ₂ O ₃ on a 3D Graphene Network: An Efficient and Recyclable Z cheme Photocatalyst. ChemPlusChem, 2020, 85, 169-175.	2.8	19
104	Searching for an Optimal Multiâ€Metallic Alloy Catalyst by Active Learning Combined with Experiments. Advanced Materials, 2022, 34, e2108900.	21.0	19
105	Fabrication of Complex Patterns with a Wide Range of Feature Sizes from a Single Line Prepattern by Successive Application of Capillary Force Lithography. Langmuir, 2010, 26, 14359-14363.	3.5	18
106	Control of periodic defect arrays of 8CB (4′-n-octyl-4-cyano-biphenyl) liquid crystals by multi-directional rubbing. Soft Matter, 2013, 9, 10135.	2.7	18
107	Hierarchical Ordering of Quantum Dots and Liquid with Tunable Superâ€Periodicity into High Aspect Ratio Moiré Superlattice Structure. Advanced Functional Materials, 2014, 24, 6939-6947.	14.9	18
108	Sonication-free dispersion of large-area graphene oxide sheets using internal pressure from release of intercalated carbon dioxide. Carbon, 2015, 88, 126-132.	10.3	18

#	Article	IF	CITATIONS
109	Grafting polycarbonate onto graphene nanosheets: synthesis and characterization of high performance polycarbonate–graphene nanocomposites for ESD/EMI applications. RSC Advances, 2017, 7, 45902-45910.	3.6	18
110	Highly conductive polyimide nanocomposite prepared using a graphene oxide liquid crystal scaffold. Carbon, 2020, 169, 155-162.	10.3	18
111	Highly ordered defect arrays of 8CB (4′-n-octyl-4-cyano-biphenyl) liquid crystal via template-assisted self-assembly. Journal of Materials Chemistry, 2011, 21, 18381.	6.7	17
112	Alignment of Perfluorinated Supramolecular Columns on the Surfaces of Various Self-Assembled Monolayers. Macromolecules, 2005, 38, 5152-5157.	4.8	16
113	Thermally responsive microlens arrays fabricated with the use of defect arrays in a smectic liquid crystal. RSC Advances, 2012, 2, 6729.	3.6	16
114	Formation of toroidal Li ₂ O ₂ in non-aqueous Li–O ₂ batteries with Mo ₂ CT _x MXene/CNT composite. RSC Advances, 2019, 9, 41120-41125.	3.6	16
115	Confined cavity on a mass-producible wrinkle film promotes selective CO ₂ reduction. Journal of Materials Chemistry A, 2020, 8, 14592-14599.	10.3	16
116	Hierarchical Self-Assembly of Perylene Diimide (PDI) Crystals. Journal of Physical Chemistry Letters, 2020, 11, 3934-3940.	4.6	16
117	Optical properties and characteristics of the cdse nanoparticles synthesized at room temperature. Korean Journal of Chemical Engineering, 2002, 19, 529-533.	2.7	15
118	Highly enhanced interfacial adhesion properties of steel-polymer composites by dot-shaped surface patterning. Journal of Applied Physics, 2011, 109, .	2.5	15
119	Facile Synthesis of Compositionâ€Controlled Grapheneâ€Supported PtPd Alloy Nanocatalysts and Their Applications in Methanol Electroâ€Oxidation and Lithiumâ€Oxygen Batteries. Chemistry - A European Journal, 2017, 23, 17136-17143.	3.3	15
120	Fabrication of a high-performance thin film polarizer using lyotropic chromonic liquid crystals using a high-resolution nanoscale template. Journal of Materials Chemistry C, 2017, 5, 12241-12248.	5.5	15
121	Nanoscale Wrinkled Cu as a Current Collector for High-Loading Graphite Anode in Solid-State Lithium Batteries. ACS Applied Materials & Interfaces, 2021, 13, 2576-2583.	8.0	15
122	Preparation of a chemically amplified photosensitive polyimide based on norbornene-end-capped poly(amic acid ethoxymethylester). Journal of Polymer Science Part A, 2005, 43, 5520-5528.	2.3	14
123	Micro- and nano-morphological modification of aluminum surface for adhesive bonding to polymeric composites. Journal of Adhesion Science and Technology, 2013, 27, 1625-1640.	2.6	14
124	Ultrastrong Anchoring on the Periodic Atomic Grooves of Black Phosphorus. Advanced Materials Interfaces, 2016, 3, 1600534.	3.7	14
125	Rational Design of Aminopolymer for Selective Discrimination of Acidic Air Pollutants. ACS Sensors, 2018, 3, 1329-1337.	7.8	14
126	Effect of Highly Periodic Au Nanopatterns on Dendrite Suppression in Lithium Metal Batteries. ACS Applied Materials & Interfaces, 2021, 13, 60978-60986.	8.0	14

#	Article	IF	CITATIONS
127	Key growth parameters affecting the domain structure of chemical vapor deposition (CVD)-grown graphene on nickel. RSC Advances, 2013, 3, 22909.	3.6	13
128	Highly enhanced mechanical properties of polypropylene-long carbon fiber composites by a combined method of coupling agent and surface modification of long carbon fiber. Macromolecular Research, 2014, 22, 1066-1073.	2.4	13
129	Controlling Smectic Liquid Crystal Defect Patterns by Physical Stamping-Assisted Domain Separation and Their Use as Templates for Quantum Dot Cluster Arrays. Langmuir, 2016, 32, 13418-13426.	3.5	13
130	Intact Crystalline Semiconducting Graphene Nanoribbons from Unzipping Nitrogen-Doped Carbon Nanotubes. ACS Applied Materials & Interfaces, 2019, 11, 38006-38015.	8.0	13
131	Eco-Friendly Water-Processable Polyimide Binders with High Adhesion to Silicon Anodes for Lithium-Ion Batteries. Nanomaterials, 2021, 11, 3164.	4.1	13
132	Fabrication of complex 3-dimensional patterned structures on a â^1/410 nm scale from a single master pattern by secondary sputtering lithography. Nanoscale, 2013, 5, 2358.	5.6	12
133	Polymer‣ayerâ€Free Alignment for Fast Switching Nematic Liquid Crystals by Multifunctional Nanostructured Substrate. Advanced Materials, 2015, 27, 6760-6766.	21.0	12
134	Highly Periodic Metal Dichalcogenide Nanostructures with Complex Shapes, High Resolution, and High Aspect Ratios. Advanced Functional Materials, 2017, 27, 1703842.	14.9	12
135	Graphene-based ultrafast nanofiltration membrane under cross-flow operation: Effect of high-flux and filtered solute on membrane performance. Carbon, 2021, 185, 641-649.	10.3	12
136	Hierarchical Wrinkle-Structured Catalyst Layer/Membrane Interface for Ultralow Pt-Loading Polymer Electrolyte Membrane Fuel Cells (PEMFCs). Nano Letters, 2022, 22, 1174-1182.	9.1	12
137	Nanoporous SiCOH/CxHy dual phase films with an ultralow dielectric constant and a high Young's modulus. Journal of Materials Chemistry C, 2013, 1, 3414.	5.5	11
138	Generation of Monodisperse, Shapeâ€Controlled Single and Hybrid Core–Shell Nanoparticles via a Simple Oneâ€ S tep Process. Advanced Functional Materials, 2014, 24, 841-847.	14.9	11
139	Hydrous amorphous RuO ₂ nanoparticles supported on reduced graphene oxide for non-aqueous Li–O ₂ batteries. RSC Advances, 2016, 6, 23467-23470.	3.6	11
140	Recent Developments in Nanoporous Graphene Membranes for Organic Solvent Nanofiltration: A Short Review. Membranes, 2021, 11, 793.	3.0	11
141	Electrochemical Activity Studies of Glucose Oxidase (GOx)-Based and Pyranose Oxidase (POx)-Based Electrodes in Mesoporous Carbon: Toward Biosensor and Biofuel Cell Applications. Electroanalysis, 2014, 26, 2075-2079.	2.9	10
142	Fabrication of sub-20 nm nano-gap structures through the elastomeric nano-stamp assisted secondary sputtering phenomenon. Nanoscale, 2014, 6, 5953-5959.	5.6	9
143	Influence of graphene thickness and grain boundaries on MoS ₂ wrinkle nanostructures. Physical Chemistry Chemical Physics, 2018, 20, 17000-17008.	2.8	9
144	Subâ€5 nm Dendrimer Directed Selfâ€Assembly with Largeâ€Area Uniform Alignment by Graphoepitaxy. Advanced Functional Materials, 2019, 29, 1901876.	14.9	9

#	Article	IF	CITATIONS
145	Plasmonic three-dimensional dimpled array from highly ordered self-assembled liquid crystal defects. Journal of Materials Chemistry C, 2013, 1, 1434.	5.5	8
146	Long-range single domain array of a 5 nm pattern of supramolecules <i>via</i> solvent annealing in a double-sandwich cell. Nanoscale, 2018, 10, 8459-8470.	5.6	8
147	Effects of Solution Annealing on the Crystallinity and Growth of Conjugated Polymer Nanowires on a Water Substrate. Crystal Growth and Design, 2018, 18, 1261-1266.	3.0	8
148	Hierarchical Metal Oxide Wrinkles as Responsive Chemical Sensors. ACS Applied Nano Materials, 2019, 2, 5520-5526.	5.0	8
149	Selective Deposition of Copper on Self-Assembled Block Copolymer Surfaces <i>via</i> Physical Vapor Deposition. ACS Applied Materials & amp; Interfaces, 2021, 13, 52931-52937.	8.0	8
150	Patterned nano-sized gold dots within FET channel: from fabrication to alignment of single walled carbon nanotube networks. Journal of Materials Chemistry, 2011, 21, 14285.	6.7	7
151	Largeâ€Area Alignment of Supramolecular Columns by Photothermal Laser Writing. Advanced Materials, 2020, 32, 2002620.	21.0	7
152	Sulfur promotes hydrogen evolution on molybdenum carbide catalysts. Materials Advances, 2021, 2, 4867-4875.	5.4	7
153	Epitaxial Crystallization Behaviors of Various Metals on a Graphene Surface. Advanced Materials Interfaces, 2016, 3, 1500741.	3.7	6
154	Selective Functionalization of High-Resolution Cu2O Nanopatterns via Galvanic Replacement for Highly Enhanced Gas Sensing Performance. Sensors, 2018, 18, 4438.	3.8	6
155	Highly Aligned Carbon Nanowire Array by E-Field Directed Assembly of PAN-Containing Block Copolymers. ACS Applied Materials & Interfaces, 2020, 12, 58113-58121.	8.0	6
156	Highly enhanced tire performance achieved by using combined carbon nanotubes and soybean oil. Journal of Applied Polymer Science, 2021, 138, 49945.	2.6	6
157	A high-performance positive-working photosensitive polyimide: Effects of reactive end groups on the physical properties of the films. Journal of Applied Polymer Science, 2006, 102, 2180-2188.	2.6	5
158	Synthesis of fluorinated polymer gate dielectric with improved wetting property and its application to organic field-effect transistors. Macromolecular Research, 2009, 17, 646-650.	2.4	5
159	Polybenzoxazole/graphene nanocomposite for etching hardmask. Journal of Industrial and Engineering Chemistry, 2019, 75, 296-303.	5.8	5
160	Surface alignment and control of a dendritic liquid crystal in ultrathin films. Liquid Crystals, 2003, 30, 559-563.	2.2	4
161	A solution processible semiconducting polymer interlayer for blue light-emitting diodes. Nanotechnology, 2007, 18, 175608.	2.6	4
162	10 nm scale nanopatterning on flexible substrates by a secondary sputtering phenomenon and their applications in high performance, flexible and transparent conducting films. Journal of Materials Chemistry C, 2014, 2, 3527.	5.5	4

#	Article	IF	CITATIONS
163	Fabrication of polythiophene patterns through blending of a thermally curable polythiophene with poly(methyl methacrylate) and selective thermal curation. Chinese Journal of Polymer Science (English Edition), 2017, 35, 422-433.	3.8	4
164	Searching for an Optimal Multiâ€Metallic Alloy Catalyst by Active Learning Combined with Experiments (Adv. Mater. 19/2022). Advanced Materials, 2022, 34, .	21.0	4
165	Polymeric photoacid generators for direct photochemical modification of surface. Polymers for Advanced Technologies, 2008, 19, 237-243.	3.2	3
166	Highly robust SiCOH/mesoporous SiO2 ultralow dielectric films with heterostructures. RSC Advances, 2014, 4, 28409-28416.	3.6	3
167	Mapping Graphene Grain Orientation by the Growth of WS ₂ Films with Oriented Cracks. Chemistry of Materials, 2020, 32, 7484-7491.	6.7	3
168	Dendritic growth in a two-dimensional smectic E freely suspended film. Molecular Systems Design and Engineering, 2020, 5, 815-819.	3.4	3
169	Fabrication of Highly Monodisperse and Small-Grain Platinum Hole–Cylinder Nanoparticles as a Cathode Catalyst for Li–O ₂ Batteries. ACS Applied Energy Materials, 2021, 4, 2514-2521.	5.1	3
170	Thickness Control of Chemical Vapor Deposition-Grown Graphene Film by Oxygen Plasma Etching with Recycled Use of Ni Catalyst. Journal of Nanoscience and Nanotechnology, 2017, 17, 4907-4913.	0.9	2
171	Long-Range alignment of liquid crystalline small molecules on Metal-Organic framework micropores by physical anchoring. Journal of Industrial and Engineering Chemistry, 2022, 105, 378-383.	5.8	2
172	Solution-Processable Graphene-Silver Nanowire Hybrids as Transparent Conducting Films. Science of Advanced Materials, 2014, 6, 2304-2311.	0.7	2
173	Spatial Control of Lithium Deposition by Controlling the Lithiophilicity with Copper(I) Oxide Boundaries. Energy and Environmental Materials, 2023, 6, .	12.8	2
174	Three-dimensional SnO ₂ nanoparticles synthesized by joule heating as anode materials for lithium ion batteries. Nano Express, 2022, 3, 025005.	2.4	2
175	Orientation and Defects on a Surface of a Thin Film of a Self-assembled Supramolecular Dendrimer. Molecular Crystals and Liquid Crystals, 2004, 412, 417-424.	0.9	1
176	Generation of optical vortex array from Toric Focal Conic Domains (TFCDs). , 2012, , .		1
177	Artificial Skin: An Ultrasensitive, Viscoâ€Poroelastic Artificial Mechanotransducer Skin Inspired by Piezo2 Protein in Mammalian Merkel Cells (Adv. Mater. 13/2017). Advanced Materials, 2017, 29, .	21.0	1
178	Ultra-dense (~20 Tdot/in2) nanoparticle array from an ordered supramolecular dendrimer containing a metal precursor. Scientific Reports, 2019, 9, 3885.	3.3	1
179	Highâ€Resolution Nanopatterning: Recent Progress in Simple and Costâ€Effective Topâ€Down Lithography for â‰^10 nm Scale Nanopatterns: From Edge Lithography to Secondary Sputtering Lithography (Adv.) Tj ETQq1	120.78431	.41rgBT /Ove
180	Wafer-Scale Unidirectional Alignment of Supramolecular Columns on Faceted Surfaces. ACS Nano, 2021, 15, 11762-11769.	14.6	1

#	Article	IF	CITATIONS
181	Strong Bathochromic Shift of Conjugated Polymer Nanowires Assembled with a Liquid Crystalline Alkyl Benzoic Acid via a Film Dispersion Process. ACS Omega, 2021, 6, 34876-34888.	3.5	1
182	Patterning of Single-Walled Carbon Nanotubes Using Wet Chemical Self-Assembling and Photolithographic Technique. Materials Research Society Symposia Proceedings, 2005, 901, 1.	0.1	0
183	Enhancement in Electrical Conductivity of Transparent Single-Walled Carbon Nanotube Films. , 2007, ,		0
184	Fabrication of well-aligned SWNT arrays using colloidal self-assembly. , 2008, , .		0
185	Sensors: An Ultrastable Ionic Chemiresistor Skin with an Intrinsically Stretchable Polymer Electrolyte (Adv. Mater. 20/2018). Advanced Materials, 2018, 30, 1870140.	21.0	0
186	Gas Sensing: Scalable Superior Chemical Sensing Performance of Stretchable Ionotronic Skin via a Ï€â€Hole Receptor Effect (Adv. Mater. 13/2021). Advanced Materials, 2021, 33, 2170102.	21.0	0
187	Sea-Urchin-like Hierarchical Carbon Spheres with Conical Pores as a Three-Dimensional Lithium Host for Dendrite Suppression. ACS Applied Energy Materials, 2022, 5, 5919-5927.	5.1	0